Check for updates

Nitrogen-doped carbon nanotubes encapsulate cobalt nanoparticles as efficient catalysts for aerobic and solvent-free selective oxidation of hydrocarbons†

Xiu Lin,[a] Zhenzhen Nie,[a] Liyun Zhang,[b] Shuchuan Mei,[a] Yuan Chen,[a] Bingsen Zhang,*[b] Runliang Zhu[c] and Zhigang Liu [ID] *[a]

The selective oxidation of hydrocarbons to the corresponding ketones with solvent-free and molecular oxygen as an oxidant is of great importance in academic and industrial fields in view of economy and environment. In this respect, we present the facile synthesis and characterization of excellent catalysts comprising cobalt nanoparticles encapsulated into graphitic nitrogen-doped carbon nanotubes (Co@GCNs) *via* one-pot pyrolysis of a chelate compound containing citric acid, melamine, and $CoCl_2 \cdot 6H_2O$. The selective oxidation of ethylbenzene under molecular oxygen and solvent-free conditions is employed as a probe reaction to investigate the catalytic performance; the optimized catalyst shows the best conversion (68%) and selectivity for acetophenone (93%). Combination of the catalytic results of the control group and the different characterization methods demonstrates that high catalytic activity is due to the synergistic effect between metallic cobalt and nitrogen-doped carbon nanotubes. Moreover, the catalyst has high catalytic activity for the aerobic and solvent-free oxidation of other aryl-alkane substrates. The proposed mechanistic study illustrates that the reaction is a free radical reaction progressing through superoxide radical anions ($^{\cdot}O^{2-}$).

Introduction

Selective oxidation of organic compounds, such as alcohols, saturated or unsaturated hydrocarbons, to the corresponding high value-added alcohols, aldehydes and ketones is of crucial importance in the synthesis of chemical intermediates or fine chemicals both in laboratory and industry.[1–4] Accordingly, in the past few decades, a great deal of research have been devoted to designing and synthesizing effective catalysts for selective oxidation of organic compounds. Noble metal catalysts such as palladium, platinum, ruthenium, and gold show superior catalytic activity and selectivity for catalytic oxidation,[2,5–7] but the high price and limited reserves greatly restrict the further usage in industry. Therefore, non-noble transition metals such as Fe,

Co, Ni, Mn and Cr have attracted considerable attention, which have been designed and synthesized in order to replace noble metals.[1] As far as we know, a series of green oxidation reactions of hydrocarbons have been reported. For example, Peng *et al.* have studied the oxidation of cumene and ethylbenzene under molecular oxygen conditions,[8–11] but the catalytic performance still needs to be improved. In view of the catalytic performance, non-noble transition metal catalysts are usually inferior to noble metal catalysts, thus some additives and oxidants, including toxic metal oxides and peroxides,[12–14] are employed to enhance the catalytic activity and selectivity of the desired products. Moreover, liquid phase solvent is generally added to reaction systems,[13–17] which lead to the presence of many difficulties in products' separation, catalysts' recovery and a sharp rise in cost. Consequently, in terms of economy and green reaction process, a catalytic system with no solvent use, molecular oxygen as an oxidant, low cost, and abundant effective catalysts will be preferred for heterogeneous catalysis. Meanwhile, it provides great opportunities and challenges for commercial large-scale application.

In recent years, carbon based materials have given rise to much interest due to their desirable physical and chemical properties including low cost, abundance as well as controllable characteristics and forms.[17,18] Among the carbon based

[a] State Key Laboratory of Chemo/Biosensing and Chemometrics, School of Chemistry and Chemical Engineering, Hunan University, Changsha, 410082, China. E-mail: liuzhigang@hnu.edu.cn
[b] Shenyang National Laboratory for Materials Science Institute of Metal Research, Chinese Academy of Sciences, Shenyang, 110016, China. E-mail: bszhang@imr.ac.cn
[c] Guangdong Provincial Key Laboratory of Mineral Physics and Material Research & Development, Guangzhou Institute of Geochemistry, Chinese Academy of Sciences, Guangzhou, 510640, China
†Electronic supplementary information (ESI) available. See DOI: 10.1039/c7gc00469a

materials, graphitic nitrogen-doped carbon nanotubes (NCNTs) are widely used in various research studies because of their high catalytic performance, providing a huge opportunity for potential application of heterogeneous catalysis.[19–22] Density functional theory (DFT) revealed that nitrogen doping can tune the charge density, spin density, and energy bandgap.[23] Magnetic metal elements are extensively introduced in heterogeneous catalysis due to their unique electron properties, low cost, and easy recovery and separation.[24–26] The magnetic metal elements can also promote the formation of nitrogen-doped carbon nanotubes with nitrogen-containing precursors during the calcination.[19,27] Furthermore, metal nanoparticles encapsulated in nitrogen-doped carbon nanotubes is a novel strategy for improving the performance of the catalyst. For example, Asefa and Bao groups have reported that the encapsulation of metal nanoparticles into nitrogen-doped carbon nanotubes can effectively improve the catalytic activity of the Hydrogen Evolution Reaction (HER).[28,29] Deng *et al.* encapsulated 3d magnetic metals into nitrogen-doped carbon nanotubes through a chemical vapor deposition (CVD) method and thought that the desirable catalytic activity originated from the synergistic effects between metal and nitrogen.[28] The encapsulation of metal nanoparticles is widely researched, however, as we know, the strategy is rarely applied to selective catalytic oxidation reactions.

Citric acid, an important organic acid compound, is widely used in the food, pharmaceutical, and chemical industries due to its great industrial value and low cost. More especially, citric acid can act as a chelating agent for cationic compounds. Thus, citric acid can chelate compounds with positive charge to form a novel precipitate of chelated composites. However, although citric acid is common and low price, its use as a chelating agent and carbon source in the preparation of carbon material catalysts is scarce.

Herein, we report a facile preparation approach in which novel cobalt nanoparticles were encapsulated into graphitic nitrogen-doped carbon nanotube hybrids (Co@GCNs) through pyrolysis of chelate compounds derived from one-pot method self-assembly of inexpensive original materials of citric acid,

melamine, and $CoCl_2·6H_2O$. The presence of cobalt nanoparticles encapsulated into carbon nanotubes has been certified by HRTEM, and other characterization data are collected from SEM, BET, Raman, XRD, and XPS. The Co@GCNs exhibit an excellent catalytic performance in selective oxidation of hydrocarbons under solvent-free and molecular oxygen conditions, and significantly have higher catalytic activity and selectivity compared to other similar catalysts. To the best of our knowledge, in terms of the catalytic oxidation with no solvent use and molecular oxygen as the oxidant, this work presents higher catalytic oxidation performance compared to previous work.

Results and discussion

Fig. 1 depicts a simple synthetic pathway of the Co@GCNs. In this experiment, citric acid not only is a carbon source, but also acts as a chelating agent, which can chelate cobalt ions and positively charged melamine to form a homogeneous chelate precipitate in aqueous solution through the protonated carboxyl group. Melamine is easily decomposed at a temperature beyond 200 °C, and layered graphitic carbon nitride will be formed at a temperature up to 550 °C at a slower heating rate.[30] Furthermore, the layered graphitic carbon nitride will be quickly decomposed once the temperature is higher than 600 °C. During the pyrolysis, carbonized citric acid is condensed to a carbon skeleton so as to form carbon nanotubes.[27,31] Therefore, the calcination temperature of catalysts is varied from 500 °C to 1000 °C. The resulted samples are denoted as Co@GCNs-*x*, where *x* represents the calcination temperature.

The morphology of the materials was investigated by scanning electron microscopy (SEM). As shown in Fig. 2, a bulk graphitic carbon nitride structure has been formed after heating at 500 °C (Fig. 2a).[32] Co@GCNs-600 shows a rod like structure in which many small holes and long-channels are discovered (Fig. 2b). What's more, when the temperature is higher than
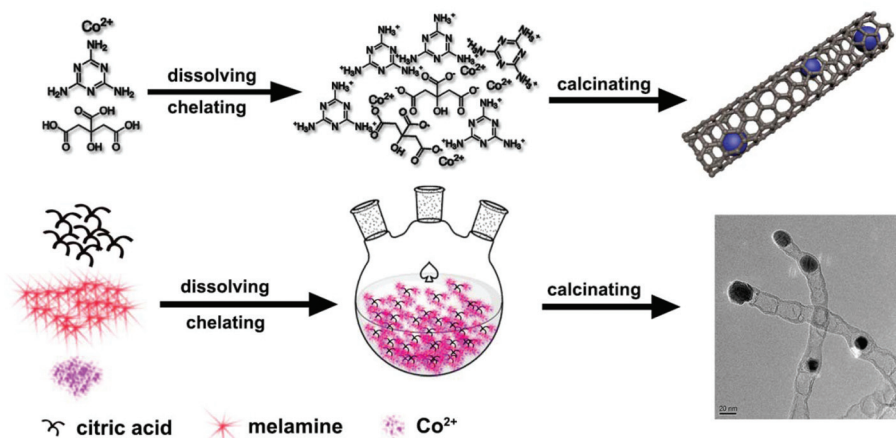

Fig. 1 Schematic illustration showing the general procedure for the synthesis of Co@GCNs.
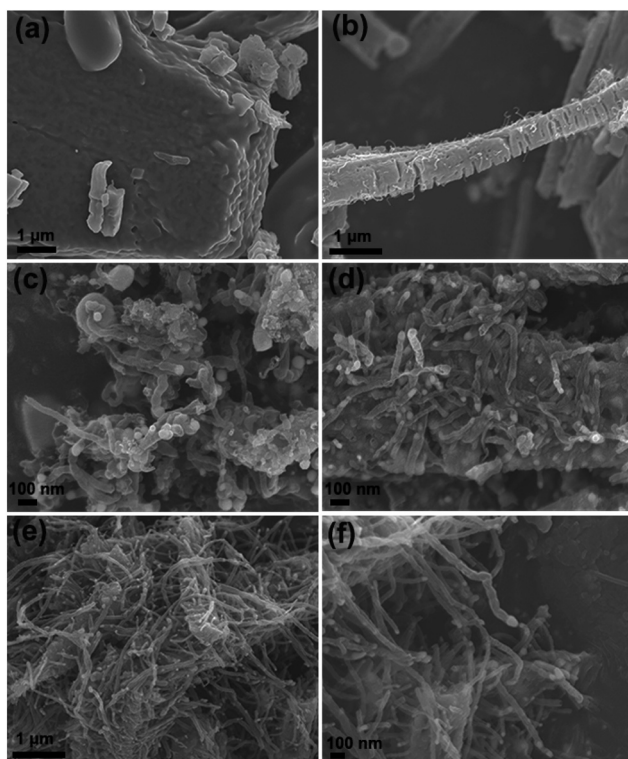
Fig. 2 SEM images of (a) Co@GCNs-500, (b) Co@GCNs-600, (c) Co@GCNs-700, (d) Co@GCNs-800, and (e, f) Co@GCNs-900.

600 °C, the materials begin to generate nitrogen-doped carbon nanotubes. With the increase of temperature, more and more carbon nanotubes are formed and the morphology becomes more and more regular (Fig. 2c–f). The size distribution of

carbon nanotubes indicates that the diameter is mainly located at 30–50 nm (Fig. S1†). It is interesting that white dots are found at the end of nitrogen-doped carbon nanotubes. The microstructure of Co@GCNs-800 was observed through high-resolution transmission electron microscopy (HRTEM). According to the HRTEM images (Fig. 3a–c), the nitrogen-doped carbon nanotubes are formed on the carbonaceous substrate presenting a bamboo-like architecture. The thickness of the wall is 4–5 nm. The metal nanoparticles with an average size of about 21 nm are encapsulated into nitrogen-doped carbon nanotubes, and some metal particles are encapsulated at the end of carbon nanotubes. So the white dots seen by SEM are the metal particles located at the end of nitrogen-doped carbon nanotubes. However, there are no carbon nanotubes formed in the Co/C-800 derived from only citric acid as a carbon source (Fig. S2b†), and the average particle size is *ca.* 81 nm, suggesting that the nitrogen-doped carbon nanotubes can encapsulate metal particles and hinder the growth. The lattice spacing of metal particles is measured to be 0.18 nm coincided with that of cubic Co and the (111) plane (Fig. 3d).[15] The elemental mappings show that N and O elements are more along with the distribution of Co elements, it may be due to the formation of some compounds among Co, N, and O elements such as Co–N, Co–O and so on (Fig. 3e). Moreover, the material without a metal exhibits thick graphite layers (Fig. S2a†), suggesting that metal nanoparticles can positively promote the formation of nitrogen-doped carbon nanotubes.

The X-ray diffraction (XRD) patterns of the Co@GCNs calcined at different temperatures are presented in Fig. 4. A weak peak at 26° is attributed to the (002) plane of graphitic carbon. Besides, three pronounced peaks at 44.2°, 51.5°, and 75.9° are ascribed to the (111), (220), and (220) reflections of cubic Co
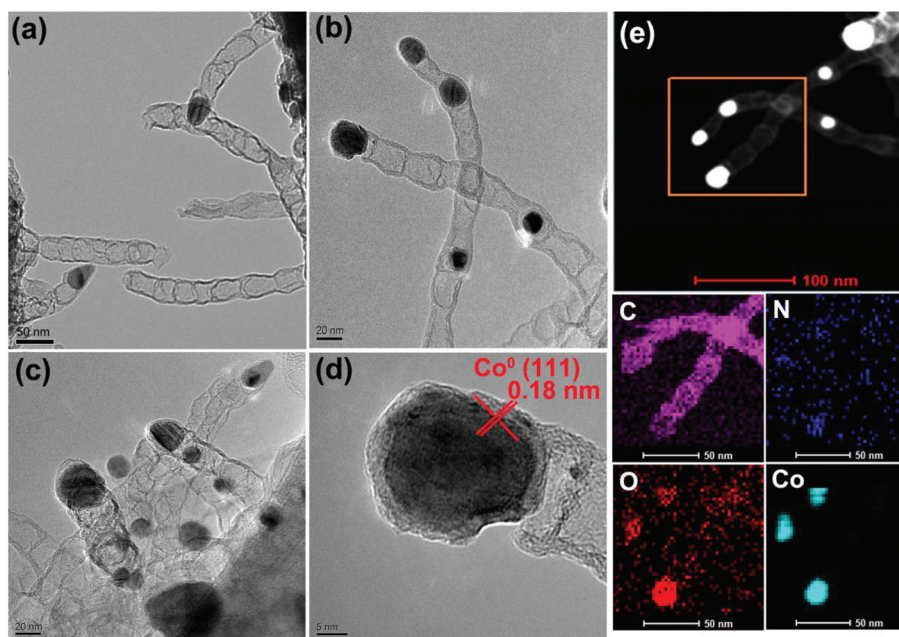

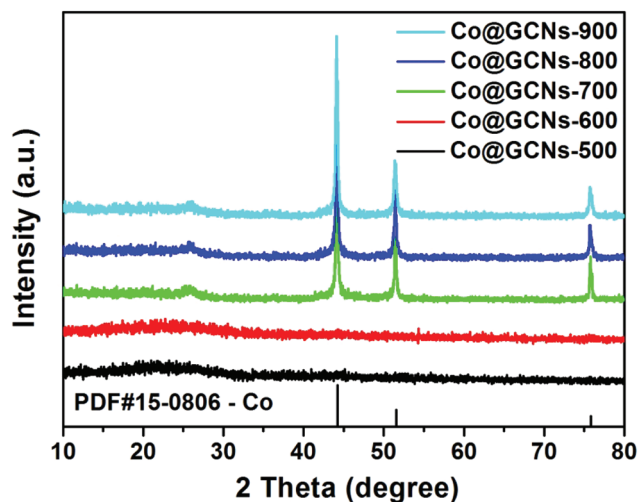**Fig. 3** HRTEM images (a–d), HAADF image and elemental mappings (e) of Co@GCNs-800.

Fig. 4 XRD patterns of Co@GCNs-500, Co@GCNs-600, Co@GCNs-700, Co@GCNs-800, and Co@GCNs-900.

Fig. 5 Nitrogen adsorption–desorption isotherms (a) and pore size distribution (b) of Co@GCNs-600, Co@GCNs-700, Co@GCNs-800, and Co@GCNs-900.

(fcc, *Fm3m* (225), JCPDS 15-0806), respectively.[15] The weak broad peak of graphitic carbon is found only in Co@GCNs-500 and Co@GCNs-600, but the others are found with narrow peaks, which may be the existence of a lower crystallization degree at low temperature. And the diffraction peak at 44.2° is apparently more intense with the increase of temperature, indicating that the crystallization of the metallic Co phase is higher at elevated temperature. Raman spectroscopy was performed to observe the electronic and structural nature of the materials (Fig. S3†). Apparently, the D band locates at 1350 cm^{-1}, which is derived from the disorder induced features caused by lattice defects, and the G band at 1587 cm^{-1} represents the in-plane vibrational modes of sp^2 carbon atoms in graphene.[33] The relative ratio of the D band to G band is more and more small along with the increase of temperature, suggesting that a higher graphite degree is formed. Moreover, a weak peak at *ca.* 670 cm^{-1} is assigned to cobalt nanoparticles.[34]

Nitrogen adsorption–desorption isotherms were obtained to investigate the textural properties of Co@GCNs. The isotherms with a large hysteresis loop in the relative pressure (P/P_0) range of 0.4–1.0 show a type IV curve according to the IUPAC nomenclature (Fig. 5a), corresponding to the characteristics of mesoporous materials with narrow pore size distribution. The large hysteresis loop suggests that a capillary condensation phenomenon has occurred in the mesoporous structure. The specific surface area and total pore volume of the materials are calculated to be as high as 232 m^2 g^{-1} and 0.37 cm^3 g^{-1} (Table 2), respectively. However, Co@GCNs-500 has a very small specific surface area, which should be due to the formation of dense graphitic carbon nitride.[32] Co@GCNs-600 shows a higher specific surface area, originating from the porous and multi-channel structure in the rod solids as evidenced in Fig. 2b. For the other materials, higher specific surface area and total pore volume are attributed to
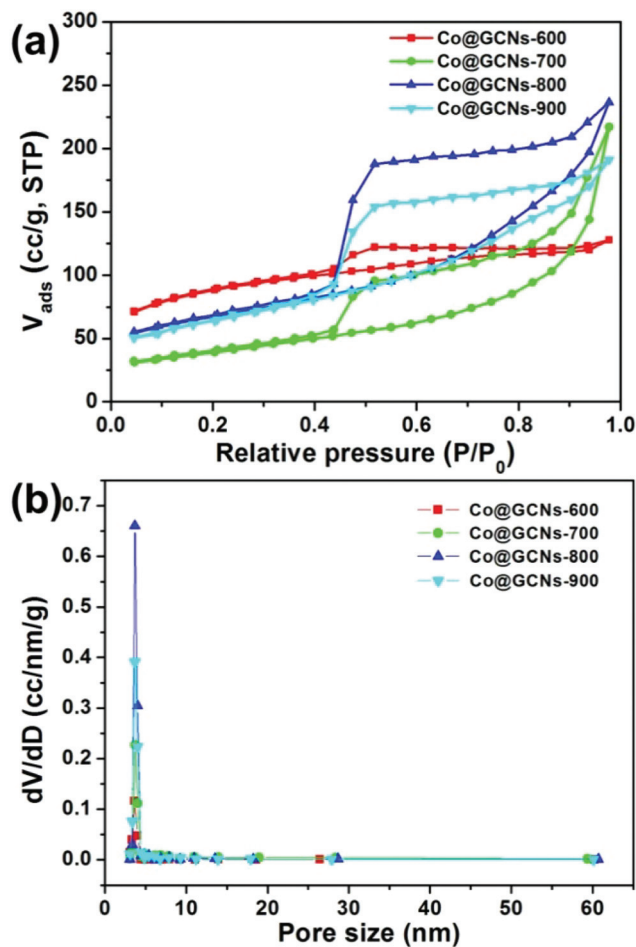
the formation of nitrogen-doped carbon nanotubes at elevated temperature. Interestingly, the pore size distribution based on the Barrett–Joyner–Halenda (BJH) formula demonstrates that the carbon nitride composites and nitrogen-doped carbon nanotubes have uniform mesopores of 3.7 nm (Fig. 5b and Table 2). Co/C-800 and MF-800 display a smaller specific surface area (Fig. S4a and b†), indicating that melamine and cobalt play an important role in preparing nitrogen-doped carbon nanotubes. The specific surface area of Co@GCNs-800 after acid treatment is significant larger than Co@GCNs-800 (Fig. S4c†), which is due to the release of space occupied by the metal.

To further investigate the elemental compositions of Co@GCN catalysts, X-ray photoelectron spectroscopy (XPS) was carried out. It can be seen from the full survey spectrum that the main elements are C, N, O, and Co in the Co@GCNs (Fig. S5†). The high-resolution C 1s XPS spectrum of Co@GCNs-800 reveals C=C, C=N & C–O, and C–N & C–O–C at 284.1 eV, 285.5 eV, and 286.9 eV, respectively (Fig. S6a†).[35,36] The high-resolution O 1s spectrum of Co@GCNs-800 is deconvoluted into three peaks with binding energies of 529.7 eV,

531.3 eV, and 532.4 eV, which can be ascribed to C–OH and/or C–O–C groups, C=O (aldehydes, ketones, lactones), and the oxygen related to cobalt oxides, respectively (Fig. S6b†).[37,38] As shown in Fig. 6a, two main peaks are located at 780 and 796 eV corresponding to the Co $2p_{3/2}$ and Co $2p_{1/2}$ binding energy, respectively. The high-resolution of Co $2p_{3/2}$ is fitted into Co^0, Co^{3+}, Co^{2+}, and satellites peaks. The peaks at 777.9 and 794.0 eV are characteristic of Co^0 in the Co 2p. It is worth noting that the content of cobalt is lower when the temperature is higher than 600 °C, it may be due to the formation of nitrogen-doped carbon nanotubes that encapsulate metal nanoparticles and make them disperse more evenly (Table 2). The content of Co^0 is significantly higher than that of the catalysts synthesized at lower temperature along with the increase of temperature, and the nitrogen-doped carbon nanotubes begin to form at elevated temperatures. Fig. 6b shows the N 1s spectra of catalysts, the N 1s can be deconvoluted into four peaks with the binding energies of 398.5, 400.3, 401.0 and 203.6 eV in agreement with the generally given range of binding energies of about 398.6, 400.5, 401.3, and 403–404 eV, which are attributed to pyridinic N, pyrrolic N, graphitic N, and *N*-oxide species, respectively.[39,40] Pyridinic N is the dominant phase in the Co@GCNs-500 and Co@GCNs-600, but graphitic N becomes the dominant phase since the temperature is higher than 700 °C and the pyrrolic N peak is disappearing, which is due to the conversion of pyridinic and pyrrolic N to graphitic N and the formation of nitrogen-doped carbon nanotubes.

The selective oxidation of ethylbenzene was chosen as the model reaction and carried out under solvent-free conditions using a certain pressure of molecular oxygen as an oxidant. The results of catalytic reactions are summarized in Table 2. The catalytic properties of these catalysts for the aerobic oxidation of ethylbenzene are determined in a high pressure reaction kettle with 0.8 MPa O_2 at 120 °C holding for 5 hours. Among the various temperatures of Co@GCNs, Co@GCNs-500 and Co@GCNs-600 show a similar and low conversion *ca.* 23% (Table 2, entries 4 and 5). However, compared with Co@GCNs-500 and Co@GCNs-600, the other catalysts have significantly improved catalytic performance for the oxidation of ethylbenzene. Co@GCNs-700, Co@GCNs-800, Co@GCNs-900, and Co@GCNs-1000 all display conversion higher than 60% and selectivity higher than 90% (Table 2, entries 6–9).

In order to thoroughly investigate the influence of catalysts, some control group experiments are performed under the same conditions. Obviously, the catalytic activity of the blank test without any catalyst is well controlled, and only 4.3% and 59.0% of ethylbenzene conversion and acetophenone selectivity are obtained (Table 2, entry 1), respectively. Furthermore, the pristine Co and CNTs are also examined and present relatively low catalytic activity (Table 2, entries 2 and 3). To study the influence of metal species, cobalt has been substituted by iron and nickel under the same conditions. It is amazing that iron and nickel catalysts exhibited poor effects in comparison with cobalt catalysts (Table 2, entries 10 and 11). As the non-cobalt metal catalysts show low catalytic activity, the metal-free catalyst prepared in the absence of a cobalt precursor shows a low catalytic activity (Table 2, entry 12). The Co@GCNs-800-AT, derived from the treatment of Co@GCNs-800 with sulfuric
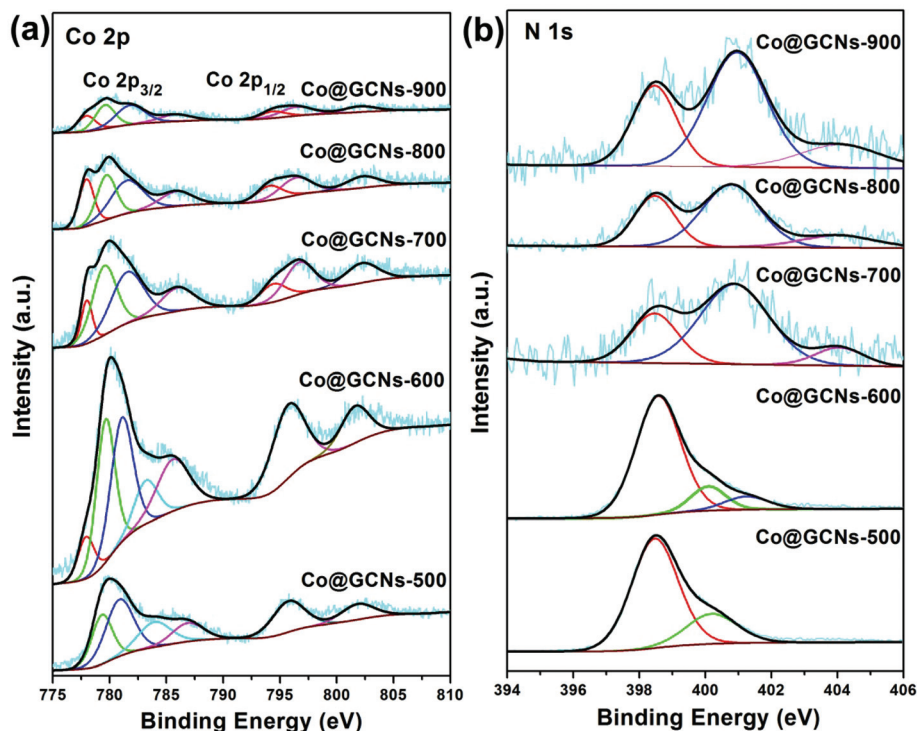

Fig. 6 High-resolution Co 2p (a) and N 1s (b) XPS spectra of Co@GCNs-500, Co@GCNs-600, Co@GCNs-700, Co@GCNs-800, and Co@GCNs-900.

acid, shows some activity in the oxidation of ethylbenzene (Table 2, entry 13), which demonstrates that the cobalt species may be the active sites in reaction. The opinion that nitrogen-containing carbon materials hold higher catalytic activity and stability for some catalytic oxidation reactions than that of non-nitrogen carbon materials has been reported by many research groups.[14,23,41,42] The Co/C-800 with only citric acid as a carbon resource possesses higher catalytic performance compared with other control groups, but it is still inferior to the nitrogen-containing catalysts (Table 2, entry 14), demonstrating that nitrogen species have an important role in enhancing the conversion of ethylbenzene. These control experiments indicate that the presence of a synergistic interaction between cobalt and nitrogen-doped carbon nanotubes plays a major role in affecting the catalytic activity of Co@GCNs-800 in the selective oxidation of ethylbenzene.

In addition to the discussion of the conversion and selectivity, the stability of Co@GCNs-800 is also investigated. As seen in Fig. S7,† the activity decreases obviously after using two times, and finally stabilizes at *ca.* 25%, this is attributed to the reason that metallic cobalt is severely oxidized during reactions (Fig. S8†). The Co@GCNs-800 after using 6 times retains the carbon nanotube structure with encapsulation of metal nanoparticles (Fig. S9†), suggesting that there is a stable nitrogen-doped carbon nanotube structure in this catalyst. However, the catalytic activity almost is recovered to the first level when the catalyst after the recycling 6 times is reheated under the same conditions. This phenomenon is due to the reduction of oxidized metallic cobalt at high temperature.
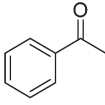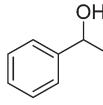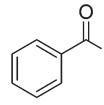
Combination of the above characterization and the catalytic reaction results suggests that metallic cobalt is the active site for reactions. Nevertheless, there is a small amount of metallic cobalt in Co@GCNs-600 (Table 1), but the catalytic activity of Co@GCNs-600 is not significantly improved compared with that of Co@GCNs-500 without metallic cobalt (Table 2, entries 4 and 5). Moreover, the pristine cobalt does not exhibit an expected catalytic effect (Table 2, entry 2). Thus, this finding demonstrates that the metallic cobalt is not the only activity site for catalytic reactions. Furthermore, there is no significant change of metallic cobalt content when the temperature higher than 700 °C, indicating that although high temperature is conducive to the reduction of cobalt, the reduction effect is

Table 1 Physical characterization and chemical compositions of various Co@GCN catalysts

Sample	S_{BET} (m^2 g^{-1})	V_{total} (cm^3 g^{-1})	D_p (nm)	Content^a (at%)				
				C	N	O	Co	Co$^{0\,b}$
Co@GCNs-500	<10	—	—	63.19	29.84	4.00	2.97	—
Co@GCNs-600	296	0.20	3.7	68.67	19.11	7.72	4.5	8.06
Co@GCNs-700	137	0.30	3.7	89.72	3.70	3.71	2.87	21.19
Co@GCNs-800	232	0.37	3.7	91.58	3.62	3.30	1.50	26.97
Co@GCNs-900	226	0.34	3.7	93.17	2.54	3.01	1.28	22.57

^{a} The contents of various elements were measured by X-ray photoelectron spectroscopy. ^{b} The relative content of Co^0 in the Co 2p.

Table 2 Catalytic activity of different catalysts for the oxidation of ethylbenzene under O$_2$ as an oxidant and solvent-free conditions

Entry	Catalyst	Conv.^{a} [%]	Sel.^{a} [%]		
			(acetophenone)	(1-phenylethanol)	(benzaldehyde)
1	—	4.3	59.0	34.5	6.5
2	Co	22.2	80.9	17.0	2.1
3	CNTs	12.7	87.4	12.0	0.6
4	Co@GCNs-500	22.5	81.0	17.6	1.4
5	Co@GCNs-600	23.7	77.8	21.5	0.7
6	Co@GCNs-700	65.4	92.3	7.7	—
7	Co@GCNs-800	68.1	93.2	6.8	—
8	Co@GCNs-900	62.3	91.3	8.7	—
9	Co@GCNs-1000	62.4	90.6	9.3	0.1
10	Fe/CN-800	16.2	72.8	24.8	2.4
11	Ni/CN-800	12.4	83.0	17.0	—
12	MF-800	12.5	78.9	18.0	3.1
13	Co@GCNs-800-AT	30.6	82.3	16.9	0.8
14	Co/C-800	49.7	84.7	14.8	0.5
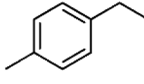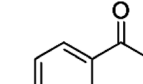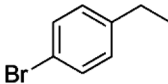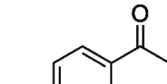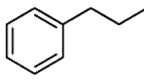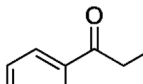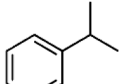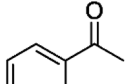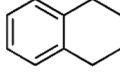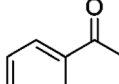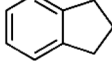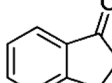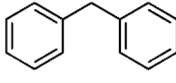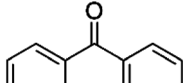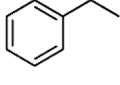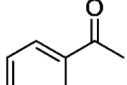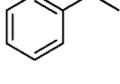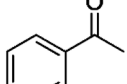
Reaction conditions: ethylbenzene (10 mL), catalyst (26 mg), O$_2$ (0.8 MPa), 120 °C, and 5 h. ^{a} Conversion and selectivity were determined by GC (dual internal standard: 1,4-dichlorobenzene and bromobenzene).

not proportional to the content of metallic cobalt. The introduction of nitrogen can facilitate the formation of nitrogen-doped carbon nanotubes and is beneficial to the encapsulation and dispersion of cobalt nanoparticles (Fig. 3), giving rise to the improvement of catalytic activity to some degree (Table 2, entry 14). According to the poor activity of pristine cobalt, carbon nanotubes as well as Co@GCNs-600 (Fig. S10†), it further demonstrates that the co-existence of metallic cobalt and nitrogen-doped carbon nanotubes can exert an excellent catalytic effect for the selective aerobic oxidation of ethylbenzene. The special structure of nitrogen-doped carbon nanotubes promotes the transfer of substrate molecules in contact with active sites.
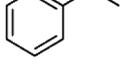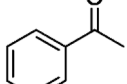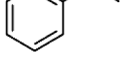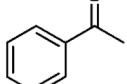
Since Co@GCNs-800 displays the best activity for the selective oxidation of ethylbenzene, it is deployed in the scope study under the same conditions. As shown in Table 3, it is seen that Co@GCNs-800 shows excellent activity for selectivity aerobic oxidation of arylalkanes to ketones. Arylalkanes containing electron donating and withdrawing functional groups show excellent conversion and selectivity to the corresponding ketones (Table 3, entries 1 and 2). The Co@GCNs-800 also exhibits superior catalytic performance for selective oxidation of *n*-propylbenzene, cumene, tetralin, indane, and diphenylmethane (Table 3, entries 3–7). Therefore, it is reasonable to say that Co@GCNs-800 is a general catalyst for selective oxidation of hydrocarbons under mild reaction conditions. In addition, several reported works about ethylbenzene aerobic oxidation are compared with this work.[43–45] Notably, the conversion 68.1% and selectivity 93.2% of Co@GCNs-800 are significantly higher than those of Co-KZrSBA-15 and $Ce_{0.5}Mn_{0.5}O_x$@500 (Table 3, entries 8 and 9). Our groups have reported a catalyst of CoNCB-2, which exhibits excellent catalytic activity (Table 3, entry 10). But Co@GCNs-800 still possesses higher conversion and selectivity under the same reaction conditions to CoNCB-2.

To gain insights into the mechanism of Co@GCN catalyzed oxidation of hydrocarbons without solvent and using O_2 as an oxidant, the oxidation of ethylbenzene in the presence of butylated hydroxytoluene (BHT) which is a kind of radical scavenger was tested (Table 3, entry 11). Notably, no acetophenone (AcPO) is produced in the presence of BHT, indicating that the reactions progress through radicals, *e.g.* the superoxide radical anion ($^•O_2^-$). As shown in Fig. 7, in the first step, O_2 gets electrons to form $^•O_2^-$ with the help of a catalyst, and ethylbenzene is absorbed onto the surface of catalyst and activated to form the phenylethyl radical (PE).[46,47] During this process, the metallic cobalt donates electrons to form positively charged cobalt ions as evidenced in Fig. S8.† Then, the PE quickly reacts with $^•O_2^-$ to form the 1-phenylethylperoxyl radical (PEPO).[11] Next, the PEPO is able to weaken the α-H bond of ethylbenzene, causing the formation of 1-phenyl-ethylhydroperoxide (PEHP) that is the main chain propagator and the most important intermediate in this process and PE.[11] In the fourth step, a reaction the same as the first step will take place and cycle. And in the fifth step, it is believed that the catalyst is favorable for the activation of the –OH bond of PEHP, leading to easier

Table 3 Aerobic oxidation of arylalkanes without solvent catalyzed by Co@GCNs-800[a]

Entry	Substrate	Product	Conv. [%]	Sel. [%]
1			78.6	89.3
2			73.7	92.2
3			55.0	82.8
4			69.2	63.0
5			67.8	62.0
6			70.7	87.6
7			78.2	95.0
8[b]			29.4	71.2
9[c]			20.3	87.0
10[d]			60.0	86.0
11[e]			—	—

[a] Reaction conditions: substrate (10 mL), catalyst (26 mg), O_2 (0.8 MPa), 120 °C, 5 h; the conversion and selectivity were determined by GC. [b] Ref. 43: catalyst of Co-KZrSBA-15, reaction conditions: ethylbenzene (10 mL), catalyst (20 mg), O_2 (1 MPa), 120 °C, 6 h. [c] Ref. 44: catalyst of $Ce_{0.5}Mn_{0.5}O_x$@500, reaction conditions: ethylbenzene (1 mmol), catalyst (30 mg), CH_3CN (5 mL), O_2 (1 MPa), 120 °C, 6 h. [d] Ref. 45: catalyst of CoNCB-2, reaction conditions: ethylbenzene (10 mL), catalyst (26 mg), O_2 (0.8 MPa), 120 °C, 5 h. [e] Reaction conditions are consistent with this work beside adding butylated hydroxytoluene (BHT) (1 mL).
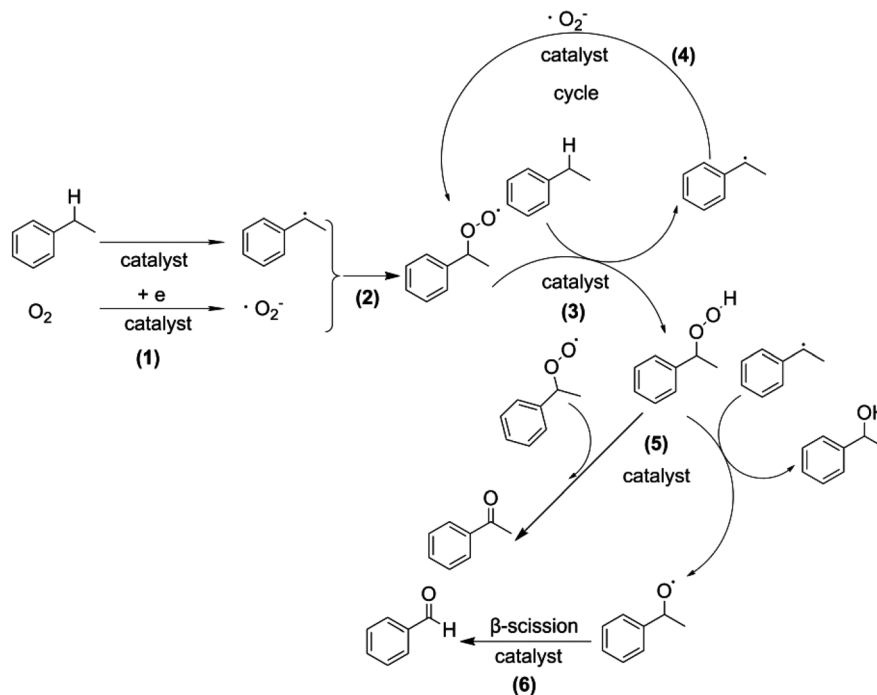
Fig. 7 Proposed mechanism for the ethylbenzene oxidation over the catalysts using O_2 as an oxidant.

reaction with PEPO to generate AcPO and higher AcPO percentage corresponding to the experimental results.[43] Simultaneously, the PEHP reacts with PE to form phenethyl alcohol (PEA) and 1-phenylethyloxy radical (PEO), however, the reaction rate of the latter is much lower than the former resulting in the low selectivity of PEA, in accordance with the experimental results.[43,48] Finally, a negligible benzaldehyde (BA) is produced due to the β-C–C cleavage of PEO.[48]

Conclusions

In summary, we have shown the facile synthesis of cobalt nanoparticles encapsulated into graphitic nitrogen-doped carbon nanotube materials (Co@GCNs) *via* one-pot thermal decomposition of chelate composites comprising citric acid, melamine, and CoCl$_2$·6H$_2$O. The Co@GCN composites show excellent catalytic performance for selective oxidation of ethylbenzene under solvent-free and molecular oxygen conditions. *Via* a series of controlled group experiments and characterization results such as HRTEM, XRD, XPS, and so on, it is found that the catalysts hold higher catalytic activity when metallic cobalt and nitrogen-doped carbon nanotubes co-exist in the system. Thus, the superior catalytic activity is assigned to the synergistic effect between metallic cobalt and nitrogen-doped carbon nanotubes. In addition, the catalyst also presents high activity for the oxidation of other arylalkanes under the same conditions. The proposed mechanism of oxidation reactions is discussed and proved to be free radical reactions. This work may provide a simple, effective, economical, and environmentally friendly catalytic system for the selective oxidation of hydrocarbons.

Experimental

Materials

Citric acid, melamine, CoCl$_2$·6H$_2$O, NiCl$_2$·6H$_2$O, FeCl$_3$·6H$_2$O, Co, and all solvents were of commercially available analytical grade and used without further purification. The CNTs were purified with HNO$_3$ in order to remove the impurities.

Catalyst preparation

Synthesis of Co@GCNs. A mixture including citric acid (1.8 g), melamine (1.2 g), CoCl$_2$·6H$_2$O (0.6 g), and deionized water (50 mL) was heated to 100 °C and stirred for 3 hours. During this process, more and more precipitate was generated and the color of the precipitate changed from red to white. After cooling down to room temperature, the obtained white precipitate was filtered and washed several times with deionized water, and then dried overnight at 80 °C in an oven. The dried solid was finely ground into powder and transferred into a crucible, directly heated at a rate of 3 °C min^{-1} to 800 °C, and kept for 2 h at this temperature under N$_2$. After that, the sample was cooled to ambient temperature, and the black product was collected and ground. The sample was denoted as Co@GCNs-800.

For comparison, the samples calcined at various temperatures were denoted as Co@GCNs-500, Co@GCNs-600, Co@GCNs-700, Co@GCNs-900, and Co@GCNs-1000. In the light of a similar preparation method, the samples in which metal salt was substituted by NiCl$_2$·6H$_2$O and FeCl$_3$·6H$_2$O were denoted as Ni@CTNs-800 and Fe@CNTs-800, respectively. The sample without a nitrogen source of melamine was named Co/

C-800. The control sample without metal ions was called metal-free (MF-800). And the Co@GCNs-800 treated with 0.5 M H_2SO_4 at 90 °C for 4 h was denoted as acid treated (Co@GCNs-800-AT).

Catalytic reaction

The selective oxidation of hydrocarbons was carried out in a 50 mL stainless steel autoclave lined with Teflon. Typically, substrates (10 mL) and catalyst (26 mg) were added into the reactor and filled with molecular oxygen (0.8 MPa). The reaction was kept at 120 °C for 5 h with continuous magnetic stirring at 900 rpm. After reaction, the catalyst was separated and recovered *via* centrifugation, and the dual internal standard of 1,4-dichlorobenzene and bromobenzene as well as the as-obtained clarified reaction mixture were added into the absolute alcohol solvent. Finally, the products were analyzed quantitatively by gas chromatography (GC) with a HP-5 ms capillary column (30 m, DF = 0.25 mm, 0.25 mm i.d.). The recovered catalyst *via* separation was washed three times with absolute alcohol, and then dried in a vacuum. The recyclability of the catalysts was investigated for the selective oxidation ability maintaining the same reaction conditions as described above. The conversion is the average results of three experiments, and error was controlled within 1%.

Characterization

Field emission scanning electronic microscopy (SEM) was performed on a JSM-6700F microscope to visualize the morphology and size of the catalysts. High-resolution transmission electron microscopy (HRTEM) was carried out on a Tecnai G2 F20 S-TWIN instrument operated at 120 kV and a Philips CM200 FEG instrument operated at 200 kV. Brunauer–Emmett–Teller (BET) specific surface areas (S_{BET}) and the total pore volume (V_{total}) were measured by N_2 adsorption–desorption analysis at 77 K and a relative pressure P/P_0 of 0.98 in a NOVA 1000e from Quantachrome Instruments. And the pore size (D_p) distribution was calculated by the Barrett–Joyner–Halenda (BJH) formula. The X-ray diffraction (XRD) pattern was collected on a Japan XRD-6100 diffractometer with the 2θ scan range between 10° and 80° using Ni-filtered Cu Kα radiation (50 kV, 10 mA). Raman spectra were obtained using a 633 nm laser on a LabRAM Aramis micro Raman spectrometer at room temperature. The surface composition was determined by X-ray photoelectron spectroscopy (XPS) using a PHI 5000C ESCA system (PerkinElmer) with an Al Kα (1486.6 eV) X-ray source, and the C 1s line (284.4 eV) was used as the reference to correct the binding energies (BE).

Acknowledgements

Notes and references

1 A. E. Shilov and G. B. Shul'pin, *Chem. Rev.*, 1997, **97**, 2879–2932.

2 L. Kesavan, R. Tiruvalam, M. H. Ab Rahim, M. I. bin Saiman, D. I. Enache, R. L. Jenkins, N. Dimitratos, J. A. Lopez-Sanchez, S. H. Taylor, D. W. Knight, C. J. Kiely and G. J. Hutchings, *Science*, 2011, **331**, 195–199.

3 J. Zhang, X. Liu, R. Blume, A. H. Zhang, R. Schlögl and D. S. Su, *Science*, 2008, **322**, 73–77.

4 D. Su, J. Wang, H. Jin, Y. Gong, M. Li, Z. Pang and Y. Wang, *J. Mater. Chem. A*, 2015, **3**, 11756–11761.

5 D. Deng, Y. Yang, Y. Gong, Y. Li, X. Xu and Y. Wang, *Green Chem.*, 2013, **15**, 2525–2531.

6 R. P. Doherty, J.-M. Krafft, C. Méthivier, S. Casale, H. Remita, C. Louis and C. Thomas, *J. Catal.*, 2012, **287**, 102–113.

7 T. Maegawa, A. Akashi, K. Yaguchi, Y. Iwasaki, M. Shigetsura, Y. Monguchi and H. Sajiki, *Chem. – Eur. J.*, 2009, **15**, 6953–6963.

8 S. Liao, Y. Chi, H. Yu, H. Wang and F. Peng, *ChemCatChem*, 2014, **6**, 555–560.

9 S. Liao, F. Peng, H. Yu and H. Wang, *Appl. Catal., A*, 2014, **478**, 1–8.

10 J. Luo, H. Yu, H. Wang and F. Peng, *Catal. Commun.*, 2014, **51**, 77–81.

11 J. Luo, F. Peng, H. Yu, H. Wang and W. Zheng, *ChemCatChem*, 2013, **5**, 1578–1586.

12 M. Jafarpour, A. Rezaeifard, V. Yasinzadeh and H. Kargar, *RSC Adv.*, 2015, **5**, 38460–38469.

13 A. Chen, Y. Yu, R. Wang, Y. Yu, W. Zang, P. Tang and D. Ma, *Nanoscale*, 2015, **7**, 14684–14690.

14 S. Yang, L. Peng, P. Huang, X. Wang, Y. Sun, C. Cao and W. Song, *Angew. Chem., Int. Ed.*, 2016, **128**, 4084–4088.

15 C. Bai, A. Li, X. Yao, H. Liu and Y. Li, *Green Chem.*, 2016, **18**, 1061–1069.

16 W. Zhong, H. Liu, C. Bai, S. Liao and Y. Li, *ACS Catal.*, 2015, **5**, 1850–1856.

17 L. L. Zhang and X. S. Zhao, *Chem. Soc. Rev.*, 2009, **38**, 2520–2531.

18 W. J. Lee, U. N. Maiti, J. M. Lee, J. Lim, T. H. Han and S. O. Kim, *Chem. Commun.*, 2014, **50**, 6818–6830.

19 C. H. Choi, S. H. Park and S. I. Woo, *ACS Nano*, 2012, **6**, 7084–7091.

20 P. Su, H. Xiao, J. Zhao, Y. Yao, Z. Shao, C. Li and Q. Yang, *Chem. Sci.*, 2013, **4**, 2941–2946.

21 J. Shui, M. Wang, F. Du and L. Dai, *Sci. Adv.*, 2015, **1**, e1400129.

22 J. Wu, R. M. Yadav, M. Liu, P. P. Sharma, C. S. Tiwary, L. Ma, X. Zou, X.-D. Zhou, B. I. Yakobson, J. Lou and P. M. Ajayan, *ACS Nano*, 2015, **9**, 5364–5371.

23 S. Wang, L. Zhang, Z. Xia, A. Roy, D. W. Chang, J.-B. Baek and L. Dai, *Angew. Chem., Int. Ed.*, 2012, **51**, 4209–4212.

24 T. Cheng, H. Yu, F. Peng, H. Wang, B. Zhang and D. Su, *Catal. Sci. Technol.*, 2016, **6**, 1007–1015.

25 Y. Chen, S. Zhao and Z. Liu, *Phys. Chem. Chem. Phys.*, 2015, **17**, 14012–14020.

26 J.-M. Yan, X. B. Zhang, T. Akita, M. Haruta and Q. Xu, *J. Am. Chem. Soc.*, 2010, **132**, 5326–5327.

27 J. Wang, Z. Wei, Y. Gong, S. Wang, D. Su, C. Han, H. Li and Y. Wang, *Chem. Commun.*, 2015, **51**, 12859–12862.

28 J. Deng, P. Ren, D. Deng, L. Yu, F. Yang and X. Bao, *Energy Environ. Sci.*, 2014, **7**, 1919–1923.

29 X. Zou, X. Huang, A. Goswami, R. Silva, B. R. Sathe, E. Mikmeková and T. Asefa, *Angew. Chem., Int. Ed.*, 2014, **126**, 4461–4465.

30 L. Liu, Y. Qi, J. Lu, S. Lin, W. An, Y. Liang and W. Cui, *Appl. Catal., B*, 2016, **183**, 133–141.

31 X.-H. Li, S. Kurasch, U. Kaiser and M. Antonietti, *Angew. Chem., Int. Ed.*, 2012, **51**, 9689–9692.

32 X. Lin, S. Zhao, Y. Chen, L. Fu, R. Zhu and Z. Liu, *J. Mol. Catal. A: Chem.*, 2016, **420**, 11–17.

33 N. L. Torad, M. Hu, S. Ishihara, H. Sukegawa, A. A. Belik, M. Imura, K. Ariga, Y. Sakka and Y. Yamauchi, *Small*, 2014, **10**, 2096–2107.

34 M. Galaburda, V. Bogatyrov, O. Oranska, V. Gun'ko, J. Skubiszewska-Zięba and I. Urubkov, *J. Therm. Anal. Calorim.*, 2015, **122**, 553–561.

35 H. Wang, Y. Zhao, F. Cheng, Z. Tao and J. Chen, *Catal. Sci. Technol.*, 2016, **6**, 3443–3448.

36 Y. Su, Y. Zhu, H. Jiang, J. Shen, X. Yang, W. Zou, J. Chen and C. Li, *Nanoscale*, 2014, **6**, 15080–15089.

37 H. T. Chung, J. H. Won and P. Zelenay, *Nat. Commun.*, 2013, **4**, 1922–1926.

38 H.-W. Liang, W. Wei, Z.-S. Wu, X. Feng and K. Müllen, *J. Am. Chem. Soc.*, 2013, **135**, 16002–16005.

39 L. He, F. Weniger, H. Neumann and M. Beller, *Angew. Chem., Int. Ed.*, 2016, **55**, 12582–12594.

40 Z. Ma, H. Zhang, Z. Yang, G. Ji, B. Yu, X. Liu and Z. Liu, *Green Chem.*, 2016, **18**, 1976–1982.

41 L. Chen, B. Huang, X. Qiu, X. Wang, R. Luque and Y. Li, *Chem. Sci.*, 2016, **7**, 228–233.

42 H. Liu, L. Chang, C. Bai, L. Chen, R. Luque and Y. Li, *Angew. Chem., Int. Ed.*, 2016, **55**, 5019–5023.

43 S. Shi, C. Chen, M. Wang, J. Ma, J. Gao and J. Xu, *Catal. Sci. Technol.*, 2014, **4**, 3606–3610.

44 P. Zhang, H. Lu, Y. Zhou, L. Zhang, Z. Wu, S. Yang, H. Shi, Q. Zhu, Y. Chen and S. Dai, *Nat. Commun.*, 2015, **6**, 8446–8455.

45 Y. Chen, L. Fu, Z. Liu and Y. Wang, *ChemCatChem*, 2016, **8**, 1782–1787.

46 X. Cui, Y. Li, S. Bachmann, M. Scalone, A.-E. Surkus, K. Junge, C. Topf and M. Beller, *J. Am. Chem. Soc.*, 2015, **137**, 10652–10658.

47 D. Bégin, G. Ulrich, J. Amadou, D. S. Su, C. Pham-Huu and R. Ziessel, *J. Mol. Catal. A: Chem.*, 2009, **302**, 119–123.

48 U. Neuenschwander and I. Hermans, *J. Catal.*, 2012, **287**, 1–4.